IOP Publishing | Astro Ltd
Laser Physics Letters
Laser Phys. Lett. **15** (2018) 045602 (4pp)
https://doi.org/10.1088/1612-202X/aa9f68

Letter

Raster-scan optoacoustic angiography reveals 3D microcirculatory changes during cuffed occlusion

Pavel Subochev, Anna Orlova, Ekaterina Smolina, Aleksey Kirillov, Natalia Shakhova and Ilya Turchin

Institute of Applied Physics RAS, 46 Ulyanov Street, Nizhny Novgorod 603950, Russia

E-mail: Pavel.Subochev@gmail.com

Received 23 November 2017, revised 30 November 2017
Accepted for publication 1 December 2017
Published 22 February 2018

Abstract

Acoustic resolution photoacoustic microscopy at the optical wavelength of 532 nm was used to investigate the functional reaction of blood vessels of healthy human skin during cuffed venous occlusion. The high bandwidth of the polyvinilidene difluoride detector provided the opportunity for raster-scan optoacoustic angiography of both the superficial and deep plexuses at the high resolution of 35/50 microns (axial/lateral). A reversible increase of blood supply in the microcirculatory bed during occlusion was revealed.

Keywords: photoacoustic microscopy, raster scan optoacoustic angiography, cuffed venous occlusion

(Some figures may appear in colour only in the online journal)

1. Introduction

Acoustic resolution photoacoustic microscopy (AR-PAM) is a raster-scan imaging technique based on the focused ultrasonic detection of wideband optoacoustic (OA) transients thermoelastically induced by nanosecond laser pulses in light-absorbing tissue chromophores [1, 2]. The most cost-effective application of *in vivo* AR-PAM imaging is in OA angiography at optical wavelengths corresponding to the absorption band of hemoglobin, allowing high contrast visualization of microcirculatory beds at up to 2 millimeter depths.

OA angiography can be performed on human skin [3] for the investigation of blood vessel reactions during different functional tests, such as cuffed occlusion. The characteristics of the vascular response to such occlusion can be interpreted as diagnostic criteria for several cardiovascular diseases. The functional response of vasculature to occlusion has previously been studied using optical methods, such as laser Doppler flowmetry for the investigation of blood flow [4] and optical diffuse spectroscopy [5] for the monitoring of blood flow, blood oxygen saturation and blood content. However, these purely optical methods suffer from low spatial resolution, as compared to hybrid AR-PAM technique.

The first successful application of AR-PAM as a method to control the functional state of the vessels during arterial occlusion was reported in [6]. Using two optical wavelengths, the authors [6] performed 2D OA monitoring of the relative oxygen saturation of the capillary vessels, which decreased during periods of arterial occlusion and temporarily increased following the occlusion. Implementing 2D AR-PAM imaging with 70 μm lateral resolution and 54 μm axial resolution at a single 570 nm laser wavelength (isosbestic point for hemoglobin) authors [6] observed a reduction of the OA signal during the occlusion and an increase in the OA signal after the occlusion in the region of the superficial capillaries. Our study, with improved spatial resolution, is devoted to functional 3D AR-PAM imaging of the hemodynamic changes during venous occlusion.

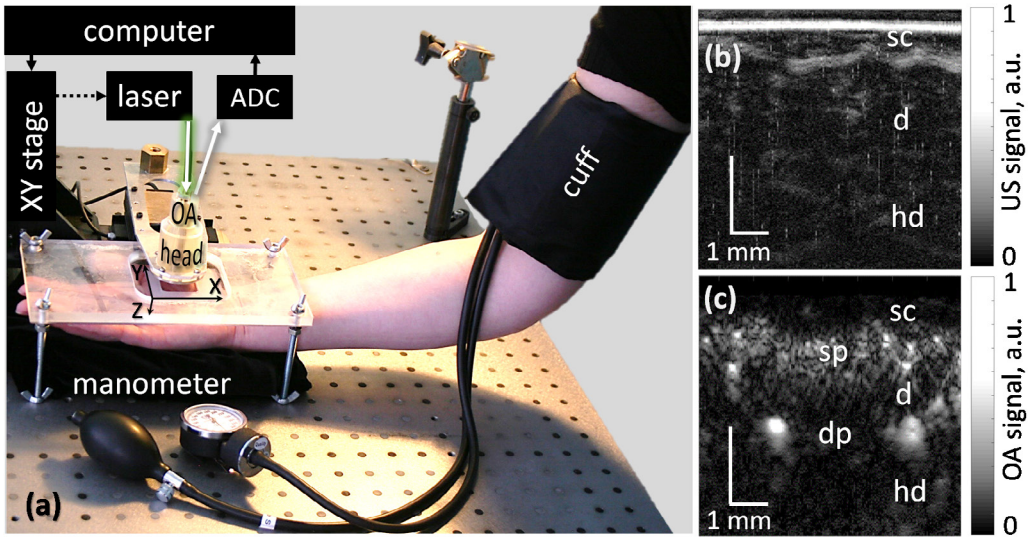

Figure 1. Raster-scan optoacoustic angiography of the human palm during cuffed occlusion. (a) Photograph of the experimental setup based on an AR-PAM microscope [7]; (b) and (c) US and OA B-scans of the human palm; sc—stratum corneum, sp—superficial plexus, d—dermis, dp—deep plexus, hd—hypoderma.

2. Materials and methods

2.1. Experimental setup for AR-PAM angiography

Figure 1 presents the setup for raster-scan optoacoustic angiography during cuffed occlusion, based on a previously developed AR-PAM system [7]. The lateral/axial OA resolution of 50 μm/35 μm was provided by the focal spot of a 35 MHz polyvinylidene fluoride (PVDF) detector with a 30 MHz bandwidth, $F = 6.8$ mm focal distance, and 0.6 numerical aperture. The scanning OA head (figure 1(a)) was mounted on two computer-driven M-664 stages performing consecutive lateral steps ($\delta x = \delta y = 20$ μm) within the lateral scanning area ($\Delta X = \Delta Y = 4$ mm). The low-jitter input of the laser Wedge HB 532 (BrightSolutions, Italy) was triggered by the scanning stages and provided optical pulses at a wavelength of 532 nm (isosbestic point for hemoglobin) with 1.4 ns duration and a power of 1 mJ. The average radiant exposure at the palm surface was 5 mJ cm^{-2}, complying with the ANSI Z136.1 standard for laser safety.

OA A-scans corresponding to discrete XY positions of the scanning head were recorded by a 16 bit analog-to-digital converter (ADC), a CSE1622 (Gage, USA), at 200 MS s^{-1} corresponding to a $\Delta z \sim 7.6$ μm spatial sampling period in the axial direction. Each laser pulse backscattered from the sample generated probing ultrasonic (US) pulses providing US A-scans delayed with respect to the OA ones and acquired by the same ADC with a 3.8 μm effective spatial sampling period [8].

2.2. Cuffed occlusion experiment

Cuffed occlusion was performed on a 20 year old healthy female volunteer in a sitting position. The lateral scanning area was selected on the palm, in the region of the thenar. The volunteer placed her hand with the palm uppermost on a supporting plate to which her wrist was fixed. Temporary occlusion was carried out using a compression cuff. The cuff was placed above the elbow joint. For the purpose of dosing the compression force, the pressure of the air pumped into the cuff was maintained at a value 60 mm Hg higher than the pre-measured systolic pressure of the volunteer [9]. The study was conducted before compression, then 5 min from its commencement and, again, immediately after deflation of the cuff. It should be noted, that the compression period was extended compared to standard cuff occlusal tests (normally the clamping time is 1.5–2 min) due to the prolonged (~5 min) OA scanning time needed to obtain an image with 250 × 250 A-scans.

2.3. Image processing

After the acquisition of the OA and US data, three post-acquisition algorithms were used to improve the resulting OA angiography images. In the first step, the *XZ* US B-scans (figure 1(b)) were used for the determination of the average vertical position of the sampled surface at each scanning step in the *Y* direction. Using motion correction technique [10] the US-based vertical alignment of each *XZ* OA B-scan was then performed. After motion correction, a 2D acoustic reconstruction algorithm [11] based on the virtual point detector concept [12] was subsequently applied to every *XZ* (figure 1(c)) and *YZ* B-scan. Finally, the reconstructed OA *XYZ* data set was processed using a Frangi filter [13].

3. Results and discussion

Figure 1 represents the reconstructed US and OA B-scans of the palm surface in the thenar zone of the female volunteer. The US image (figure 1(b)) allows us to identify the different layers of skin and to determine their thickness, shape and homogeneity. The epidermal, dermal and hypodermal layers can be distinguished. The thickness of the stratum corneum is about 0.4 mm, which is typical for the thickened skin of

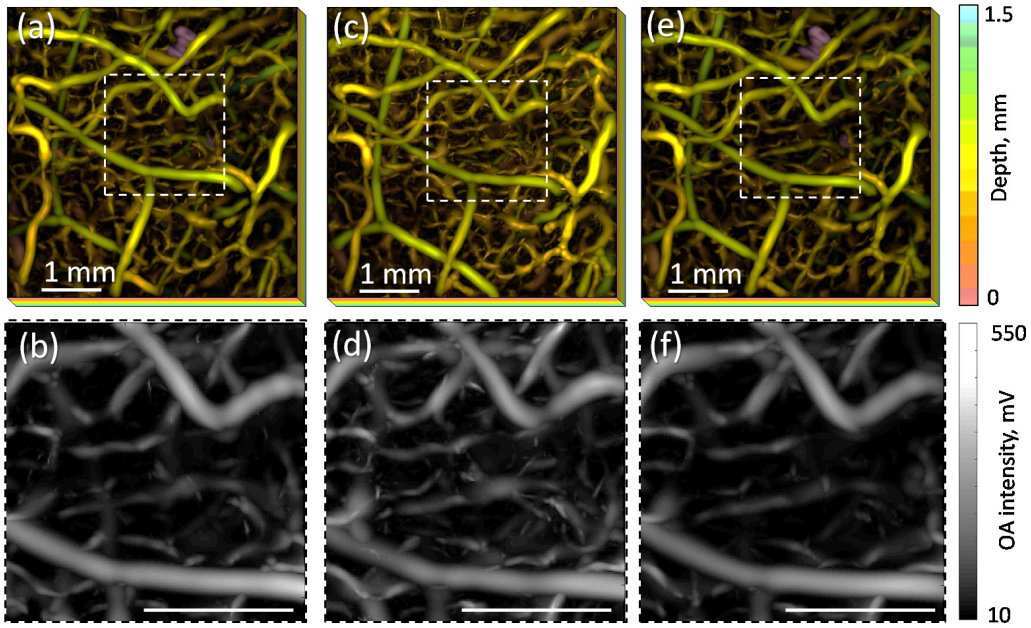

Figure 2. OA angiograms of human palm: (a) and (b) before, (c) and (d) during, (e) and (f) after cuffed occlusion. The color scale encodes the depth of the corresponding blood vessels; the gray scale represents the maximum optoacoustic intensities at the center of the imaging region, projected onto the *XY* plane.

the palm. The OA B-scan (figure 1(c)) visualizes hemoglobin-containing blood vessels as highly absorbing structures and, therefore, allows determination of their size, position and depth. According to their size and depth of occurrence, two types of vessel structures can be distinguished in the cross-sectional image (figure 1(c)): the large vessels (approximately 500 μm in diameter) located at a depth of about 1 mm from the skin surface, may be interpreted as part of the deep vascular plexus, while smaller vessels, approximately 50 μm in diameter, lying near (0.5 mm) the surface, may be identified as part of the superficial vascular plexus. Comparison with ultrasound images confirms the position of the detected vascular structures. The superficial plexus is located in the papillary dermis directly under the epidermis. The deep plexus is located in the lower zone of the reticular dermis just above the hypodermis [14]. It should be noted, that the OA images do not show all the structures of the vascular network of the skin, since vessels located closer than 50 μm to each other cannot be resolved due to the limited lateral spatial resolution.

Figure 2 shows the microvascular organization of the thenar zone of the same volunteer before (figures 2(a) and (b)) during (figures 2(c) and (d)) and after (figures 2(e) and (f)) cuff occlusion. The depth of the individual blood vessels (figures 2(a), (c) and (e)) is encoded using different colors (orange superficial vessels and green deep vessels). The relative intensities of the OA signals within the central dotted regions (figures 2(b), (d) and (f)) are represented in grayscale.

Figure 2(c) represents the changes in 3D organization of the blood vessels caused by the interruption of venous blood outflow. The observed changes are characterized by increased OA signal intensity connected with the redistribution of hemoglobin within the microcirculatory bed of the skin. The observed effect was most pronounced in the smallest vessels identified as being in the superficial plexus. After the end of occlusion, restoration of the initial parameters of the blood vessels was observed.

The elevation of blood content during venous occlusion has already been demonstrated using optical methods. Near-infrared spectroscopy [9, 15] has revealed a 1.5-fold increase in hemoglobin concentration in the skin and a 2-fold increase in muscle. In our study using OA, changes in the blood content of the skin vascular network were demonstrated. Additional information about the functional state of the blood vessels during occlusion can be obtained by multispectral optoacoustic tomography [16] for monitoring oxygenation, while optical coherence microangiography [17] provides for the characterization of blood flow.

4. Conclusion

Raster-scan AR-PAM imaging at an optical wavelength of 532 nm was used for OA angiography of the human skin. To realize complementary US measurements, our system used the photons backscattered from the sample towards an acoustic detector. Simultaneously acquired US data was essential for understanding the anatomical position of the vessels and allowed the elimination of motion artefacts from the 3D OA data. OA angiograms allowed characterization of the hemodynamic response during cuff venous occlusion. The improved spatial resolution of our 3D AR-PAM imaging system allowed observation of the accumulation of hemoglobin in the superficial vascular plexus due to the temporal termination of venous blood outflow. Raster-scan OA angiography could therefore provide the useful tool for studying the functional changes of cutaneous microcirculation in the diagnosis of vascular diseases.

Acknowledgments

This work was supported financially by the Russian Science Foundation (project #14-15-00709). Dr Pavel Subochev was partly supported by a Scholarship of the President of the Russian Federation (project #SP-3196.2016.4). The authors are grateful to Irina Mikhaylova and Maxim Prudnikov for their assistance during the *in vivo* experiments.

Disclosure

The authors can confirm that they have no conflicts of interest.

References

[1] Zhang H F, Maslov K, Stoica G and Wang L V 2006 *Nat. Biotechnol.* **24** 848–51
[2] Omar M, Rebling J, Wicker K, Schmitt-Manderbach T, Schwarz M, Gateau J, López-Schier H, Mappes T and Ntziachristos V 2017 *Light Sci. Appl.* **6** e16186
[3] Schwarz M, Buehler A, Aguirre J and Ntziachristos V 2016 *J. Biophoton.* **9** 55–60
[4] Addor G, Delachaux A, Dischl B, Hayoz D, Liaudet L, Waeber B and Feihl F 2008 *Physiol. Res.* **57** 685–92
[5] Yu G, Durduran T, Lech G, Zhou C, Chance B, Mohler E R and Yodh A G 2005 *J. Biomed. Opt.* **10** 024027
[6] Favazza C P, Cornelius L A and Wang L V 2011 *J. Biomed. Opt.* **16** 026004
[7] Subochev P 2016 *Opt. Lett.* **41** 1006–9
[8] Subochev P, Fiks I and Frenz M 2016 *Laser Phys. Lett.* **13** 025605
[9] Casavola C, Paunescu L A, Fantini S and Gratton E 2000 *J. Biomed. Opt.* **5** 269–76
[10] Schwarz M, Garzorz-Stark N, Eyerich K, Aguirre J and Ntziachristos V 2017 *Sci. Rep.* **7** 10386
[11] Jaeger M, Schüpbach S, Gertsch A, Kitz M and Frenz M 2007 *Inverse Problems* **23** S51
[12] Li M-L, Zhang H F, Maslov K, Stoica G and Wang L V 2006 *Opt Lett.* **31** 474–6
[13] Oruganti T, Laufer J G and Treeby B E 2013 *Proc. SPIE* **8581** 85811W
[14] Weller R P, Hunter J A, Savin J A and Dahl M V 2013 Medical treatment of skin disease *Clinical Dermatology* 4th edn (Malden, MA: Blackwell Publishing) pp 364–70
[15] Nagashima Y, Yada Y, Hattori M and Sakai A 2000 *Int. J. Biometeorol.* **44** 11–9
[16] Deán-Ben X L and Razansky D 2013 *Photoacoustics* **1** 68–73
[17] Matveev L A, Zaitsev V Y, Gelikonov G V, Matveyev A L, Moiseev A A, Ksenofontov S Y, Gelikonov V M, Sirotkina M A, Gladkova N D and Demidov V 2015 *Opt Lett.* **40** 1472–5